

IMPERIAL COLLEGE OF SCIENCE,
TECHNOLOGY AND MEDICINE

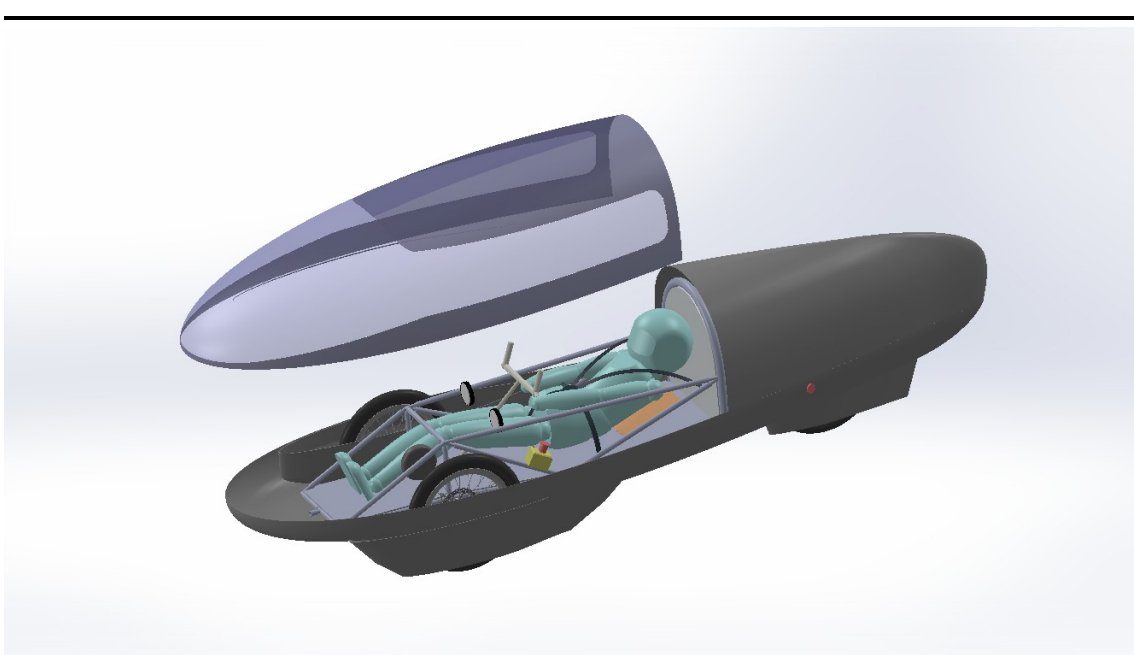
DEPARTMENT OF AERONAUTICS

MENG AERONAUTICAL ENGINEERING

AERO96005 - GROUP DESIGN PROJECT

Shell Eco-marathon 2020

Aerodynamic Design of Battery-Electric Prototype Class



Student:

Xerxes CHONG

CID:

01389744

Supervisor:

Prof. Joaquim PEIRÓ

Project Coordinator:

Prof. Joaquim PEIRÓ

June 15, 2020

Abstract

This report focuses on the validation and set-up of 3D CFD simulations of a SEM vehicle using the CD-adapco STAR-CCM+ software. Validation was performed using the Ahmed Body 25° model and a low -2.7% error in Drag Coefficient was achieved for the 3D validation. 2 design iterations were performed that investigate wheel fairing design and vehicle lengths on aerodynamic performance. The resulting design had a $C_{DA} = 0.0399$ and a positive $C_{LA} = 0.0608$. Compared to the first iteration, this was an increase in C_{DA} of 3.4% and a change from a neutral lift to a positive lift configuration. The lessons learnt and future considerations for CFD simulations are discussed at the end of the report

Contents

List of Figures

List of Tables

1 Executive Summary

2 CFD Validation 1

2.1	Need for CFD	1
2.2	Need for Validation	1
2.3	Ahmed Body	1
2.4	Problem Definition and Boundaries	2
2.5	Mesh Settings and Volumes of Refinement	3
2.6	Physics Settings	4
2.7	Convergence	5
2.8	Results	6

3 Preliminary Designs 7

3.1	SEM simulation	7
3.2	Mesh Independence Study	7
3.3	IRG Aeroshell Appraisal	8
3.4	Iteration One	8
3.5	Iteration Two	9

4 Final Design 10

4.1	Results	10
4.2	Future CFD Considerations	11

5 Conclusion 12

References 13

A Appendix 14

A.1	Ahmed Body	14
A.2	Simulation setup dimensions	15
A.3	Mesh Control	16
A.4	Ahmed Body Validation Plots	17
A.5	SEM Simulation	20
A.6	Mesh Independence	22

List of Figures

1	<i>The computational domain for the validation of the Ahmed Body</i>	2
2	<i>Periodic oscillations about a mean value observed in the Drag Coefficient from a steady $k - \omega$ SST simulation of the Ahmed Body</i>	5
3	<i>The side and rear wake profile from the simulation matches that from a Large Eddy Simulation from [1]</i>	6
4	<i>Plots showing the variation of C_L and C_D with increasing cell count</i>	7
5	<i>A line integral convolution (LIC) of the velocity vectors was taken at three locations from the nose of the vehicle</i>	11
6	<i>The Ahmed Body's dimensions and placement in the computational domain</i>	14
7	<i>Dimensions for Computational Domain and the Volume of Refinement as seen from the front</i>	15
8	<i>Dimensions for Computational Domain and the Volume of Refinement as seen from the side</i>	15
9	<i>The degree of control over mesh refinement afforded by volumetric control is clearly demonstrated in the second row of images. The first row demonstrates how inconsistent and unpredictable the constant growth rate method can be [2]</i>	16
10	<i>Drag Coefficient plot for the 4 settings</i>	17
11	<i>Lift Coefficient plot for the 4 settings</i>	18
12	<i>Residual plot for the 4 settings</i>	19
13	<i>The computational domain for all SEM simulations</i>	20
14	<i>The volume mesh of the SEM simulations</i>	20
15	<i>Prism Layers on the surface of the SEM model</i>	21
16	<i>Wall $Y+$ values that are within range across the model</i>	21
17	<i>Plots showing the variation in total run time to convergence for the SEM setup during mesh independence test</i>	22

List of Tables

1	<i>List of main components and a brief description</i>	1
2	<i>List of key parameters and their values</i>	2
3	<i>Summary of boundary types for Ahmed Body simulation</i>	3
4	<i>Effect of changing turbulence model and solver state on drag coefficient prediction</i>	4
5	<i>Validated settings</i>	6
6	<i>Difference in speed of simulation at mesh independent and dependent cell count. Simulations performed on a 4 core Intel i7-7500U CPU</i>	8
7	<i>Comparison of drag coefficient predictions for the IRG 2019 shell</i>	8
8	<i>Results of the simulations performed on the 3 wheel fairing designs</i>	9
9	<i>Results of the simulations performed on different vehicle lengths</i>	9
10	<i>Results of mesh-independent simulations of final (red) and first design. Also included are the results of the final shell without the scaling performed</i>	10
11	<i>Mesh Refinement Methodologies [3]</i>	16

1 Executive Summary

Technical Director and Project Coordination

The objective of the Shell Eco-Marathon Group Design Project was to design a prototype electric battery vehicle to compete and ultimately win the Shell Eco-Marathon competition at Mercedes-Benz World racetrack in July 2020, with a budget of £8000. Even though the competition for 2020 has been cancelled, this design project provides IRG a vehicle platform that can be built upon for the next round of competitions (summer of 2021 as of now). The proposed design has two wheels at the front and one at the rear, to accommodate a tear-drop shape low drag aeroshell. The vehicle has Front-wheel steering per the SEM regulations and a rear-wheel drive. The vehicle's power plant is a 180W Brushless Maxon motor, powered by 8 Samsung INR18650-25R cells. The vehicle has a space frame style CFRP chassis and an integrated aluminium 2090 T83 roll bar. The aeroshell is a non-load bearing structure made up of custom top, side, and under-body profiles with integrated wheel fairings. It is constructed from CFRP and a transparent Polycarbonate canopy to maximise driver visibility. The teams choice of tyre for the design was the Michelin 4575R16, these offer the lowest rolling resistance coefficient of any tyre available on the market and are manufactured specifically for this competition. The final mass estimation without the driver is 25.49 kg. The vehicle was designed around the selection of a 10th percentile female driver, of mass 50 kg when wearing full race gear.

A performance metric was constructed to analyse the sensitivity of the vehicle performance to varying key parameters, with a final performance estimation of 1141 km/kWh. This performance estimate exceeds our target of 900 km/kWh. We acknowledge that our performance metric only models the ideal conditions and does not consider losses due to driver error. This design project was solely based on theoretical work and for future adaptation, we propose experimental testing of individual components to IRG. Based on the sensitivity analysis of the final design the team believes the vehicle's aerodynamics is the area where the largest performance gains could be made. As such we advise IRG to take advantage of our vehicle's modular design which allows the aeroshell to be easily replaced without requiring a large redesign of the vehicle to build and rigorously test different aeroshells.

Please refer to the report by Davide Vaccaro for detailed information on 'Technical direction and project coordination'.

Rules and Regulations Compliance

Without appropriate regulation compliance the design could be disqualified from the competition at the technical inspection. The purpose of the rules and regulation compliance team was to ensure the vehicle produced is fully compliant with the rules and regulations set out by the organiser, Shell, and also compliant with the IRG internal rules surrounding budget and other constraints e.g. driver dimensions. The

rules and regulations for Shell are documented in 2 rule books which can be found online. By populating a spreadsheet the rules could be broken down between the sub-teams and managed accordingly.

The first focus for the compliance team were the conceptual design regulations, namely the dimensions. Once this was completed the focus shifted onto the sub-team specific rules. These were regularly checked for compliance as the design progressed.

Any discrepancies with the design or unclear rules were managed appropriately by discussing the problem with Imperial Racing Green and coming to a joint conclusion. The vehicle was deemed to be fully compliant by the end of the design process.

Please refer to the report by Emily Middlebrough for detailed information on ‘Rules and Regulations Compliance’.

Packaging

Integration of different sub components is an essential aspect for the success of the project and it is the role of Packaging to communicate efficiently between different sub-teams. The integration of the car relied upon a constantly active line of communication between each sub-team and the packaging team. When a change was made by any sub-team, to ensure the smooth running of the project, the packaging team were required to use their ‘big-picture’ view of the project to quickly and efficiently communicate any knock-on effects to other sub-teams.

At the start of the project the team helped with the outlining of the conceptual design by considering the possible configurations of car. The packaging team helped the initial decision to go with a three-wheel configuration with two front wheels, a single rear wheel, front wheel steering and rear wheel drive. As the project developed the packaging team worked closely with the different sub teams to assist them in any major design decisions, such as the steering system, power train mounting and window sizing. In order to make any changes clear to the whole team, a SolidWorks drawing was made easily available for any team member to reference and gather any required dimensions. A centre of gravity chart and a version control system documenting different versions of design is also maintained throughout the project.

Please refer to the reports by David Simmonds and Zijun Liao for detailed information on ‘Packaging and Integration’.

Aerodynamics

The Aerodynamics team had the task of designing an aerodynamically competitive shell whilst making sure to comply with race regulations and the vehicle’s packaging constraints. For this reason, much time was spent working with sub-teams in charge of the chassis, wheels, steering, packaging and driver environment to produce

a vehicle concept that would allow a major aerodynamic improvement compared to the current IRG design.

With much inspiration taken from 2 world record holding contenders, a vehicle with a relatively high ground clearance and most importantly, wheel fairings, was produced. In addition to a custom top view “teardrop” airfoil shape and long slender profiles for the side view and wheel fairings, the final vehicle showed much better drag characteristics than the previous IRG design. The shell is also expected to improve the visibility issues previously experienced, with the whole front half of the car’s canopy made fully out of transparent polycarbonate material using only tinting to reduce direct sunlight on the driver and the remainder of the shell produced out of carbon fiber reinforced epoxy resin.

The final drag coefficient is estimated to be around 0.075 deemed to be highly competitive amongst previous top contenders. However, there is still work to be done in the future including a reworked fairing and under-body integration to ensure neutral lift, improved CAD to allow tighter packaging around the roll bar and wheels for a smaller frontal area and finally, wind tunnel testing to validate the results seen in CFD simulations.

Please refer to the reports by Toby Bryce-Smith, Xerxes Chong, Cedric van Den Berg and Michal Wietlicki for detailed information on ‘Aerodynamics’.

Drive Train

The drive train includes motor, transmission, tyre and wheel. Motor selection began with power requirement estimation using initial sizing data provided by Packaging and Aero Teams. A preliminary mission profile was designed with help from Vehicle Dynamics Team. An algorithm was developed with MATLAB which utilised technical data from manufacturer to compute energy usage for shortlisted motors during the race. Through comparison of mileage, mass and optimal gear ratio, Maxon 574741 was selected. The predicted mileage using primary mission profile was 1347.5km/kWh, with optimal gear ratio of 4.3. Motor data was sent to Electronics and Vehicle Dynamics Teams for race strategy analysis. Final mileage achieved was 1141.15 km/kWh.

For transmission, shaft design was chosen, as it was light and offered very high power transmission efficiency of 99%. Given optimal gear ratio of 4.3 no planetary gear or multi-step transmissions were required. The final design consisted of a woven CFRP shaft perpendicular to the rear axle connected to the motor, which would be mounted in between two chassis members at the rear of the car. Translation of the torque would be achieved by a straight bevel gear. The bevel gear was mounted to a standard bike freewheel cassette to allow the wheel to coast without overloading the motor. A frame was designed to ensure alignment of the axles, and smooth meshing of gear teeth.

Michelin Prototype 45/75R16 tyre was chosen as it had the lowest rolling

resistance coefficient of 0.00081 in all rubber-made tyres. For wheel design, customization of BMX wheel was chosen due to its high cost-effectiveness. Customized 20" Alienation TCS VANDAL rim was chosen to firmly accommodate the tyre. Shimano RS770 hubs were chosen for brake disc and gear compatibility. Other wheel parts would be purchased separately and assembled with the help of truing stand in the bike storage in the college.

Please refer to the reports by Pengchao Hu and Lorenzo Tresca for detailed information on 'Drive Train'.

Vehicle Chassis

A spaceframe chassis built upon a ladder chassis base was designed to support the driver and the components of the chassis. This is primarily based on the *Vehicle Dynamics, Driver Environment and Packaging* constraints and allows flexibility for any dimensional changes during the conceptual phase. As the design progressed, the space frame adaptation approach would be used.

The Engineer's Theory of Bending is used to analyse the deflections of the chassis base during the conceptual design phase. The cross section of the structure is chosen based on the relations between torsional loading and twist. A truss structure analysis was done to identify the optimum chassis sides and verify the effectiveness of its implementation on reducing the deflections. As the chassis structure increased in complexity, analysis was done purely based upon FEA results. Additional members were included and the diameters of the members under critical stresses and deflections were increased to improve the performance of the structure.

The final chassis structure gives a maximum deflection of 0.69 mm under static loading and a 3.97 mm maximum deflection and 2.09° rotation in the worst case of dynamic loading, which are within the requirements of the IRG team. The spaceframe will be made of roll wrapped carbon fiber tubes, assembled using Al 6082 inserts. The tubular members and the inserts will be bonded together with HexBond 870 Shimming Epoxy. The final mass of the assembled space frame is 3.24 kg and the estimated cost is £534.

Please refer to the reports by Samuel Cross, Sakishna Linganathan, Angeliki Tzola and Imran Ahmad Azhar for detailed information on the 'Vehicle Chassis'.

Loading and Crash Protection

The aim was to design crash safety structures to protect the driver from possible impact conditions of the vehicle. The lateral instability of the vehicle made roll overs the most probable form of impact. Regulations required a roll bar or panel to be constructed which could withstand a load of 700 N without significant deformation.

Industry grade techniques of pre-processing, simulations and post-processing were adopted to design an efficient Roll bar. The pre-processing stage included thorough research in material and cross-section selection, possible joining methods,

adoption of efficient 2D finite element methods to choose the optimum shape and lastly, to obtain the range of possible deflections due to different degrees of clamping. The post-processing stage came after the 3D simulations where detailed conclusions were made with respect to the complete failure analysis of the roll bar, accuracy of the 2D simplified model and the robustness of the clamping assumptions made in the 2D analysis. These steps concluded a maximum displacement of 3.8 mm with the limit set at 5 mm. Furthermore, this process assured crash protection in case of roll overs.

Other possible impact conditions were assessed i.e. driver entry and crumple zone regulations. Overall, the vehicle was concluded to be safe in case of probable crashes and possible improvements were listed to further optimise the structures.

Please refer to the report by Devanshu Ghosh for detailed information on ‘Loading and Crash Protection’.

Power and Control

The role of the Power Electronics and Control sub-team was to simulate performance of power systems and work with Powertrain and Vehicle Dynamics sub-teams to optimize component and strategy selection respectively. A model for all electronic systems in the powertrain was therefore developed and integrated with a dynamics model to simulate the vehicle’s performance throughout the race. In particular, the performance and integration of the motor controller was analyzed.

Particular focus was also placed on driver interaction with the vehicle’s power systems. An intuitive control scheme for the vehicle’s cruise control was created in order to maintain a constant speed throughout the race and improve efficiency. At request of IRG, a real-time telemetry system was also designed that would transmit sensor data from the vehicle to the team using cellular networks while serving as a central vehicle computer with control over throttle actuation, driver displays, and the aforementioned cruise control system.

Finally, the Power Electronics and control sub-team was responsible for maintaining a list of project deliverables and consulting any suggested changes with IRG to ensure their needs, as our customer, were met.

Please refer to the report by Tomas Mrazek for detailed information on ‘Power and Control’.

Braking System

Theoretically, if the driver was to follow the race strategy, brakes will not be used during the race. However, the brakes still play a big part in the competition as there will be a technical inspection test which the brakes are required to pass whilst complying with all the rules. In order to pass the braking test, the vehicle - with the driver inside – placed on a slope with an inclination of 11.3° , must remain stationary. Nevertheless, the brakes have an important role for safety and efficiency purposes.

Considering factors like speed, weight and tyre size of the brakes, a brake similar to a mountain bike brake is chosen due to the similarity in the aspects listed earlier. The selection of brake components from the market was based mostly on weight reduction and performance; in order to increase the overall performance of the car. The merits of typical bicycle brakes are assessed and Shimano BR-M8110 disc brake callipers and BL-M8100 hand brake lever are used. Meanwhile, the rotor disc will be made in house by IRG and the optimised foot pedal will be 3D printed in house using ABS due to its lower weight and price considerations. Braking power is transmitted by Shimano SM-BH90-SS Brake Hose which is routed along the chassis and steering column. The front callipers will be side mounted on the optimised brake arm and the rear brake calliper will be flat mounted like a bike. The handbrake lever will be mounted in the middle of the vertical handlebar adaptor. Overall, the performance of brake system would also depend on the installation quality and the actual brake test.

Please refer to the reports by Pok Wei Hui for detailed information on ‘Braking system’.

Suspension and Steering

Suspension was decided to not be implemented in our vehicle design, as no stability issues were experienced during the required race manoeuvres as calculated by *Vehicle Dynamics*, and potential contact of wheel fairings with the ground due to wheel travel.

The vehicle has 2 front and 1 rear wheel, and the rules dictate front wheel steering only is permitted. It is operated with a handlebar with vertical attachments at the hands for more ergonomic use, and utilising a universal joint to transmit rotation to a pitman arm. The pitman arm and tie rods operate under the chassis floor, as this is safer and less invasive to the driver with no moving connections in their compartment.

Full Ackermann steering was used to allow appropriate independent inner and outer wheel turn angles to prevent the wheels fighting and slipping. The max wheel turn angle is for the 8m radius turn test at technical inspection, a safety margin of 20% was added as our full lock angle to allow for any unpredicted behaviour of the wheels and for any mismanufacture of components and the car. The steering was modelled to have a minimum steering ratio of 1:1 for the inner wheel to provide controlled and responsive steering, whilst allowing a non-invasive turning of the handlebar and the driver.

Please refer to the report by Corey Taylor for detailed information on ‘Steering and Suspension’.

Driver Environment and Interfaces

The first task for the Driver Environment and Interfaces team was to select a suitable driver and optimise the seating position. The most important aspect for the driver was minimising weight and so a female in the lowest 10th percentile weight category was chosen. A supine seating position was selected due to the corresponding decrease in the frontal and wetted areas of the vehicle.

The next stage was to consider the driver interfaces. The steering wheel, being the centre of the interface, was designed to be a compact handle bar to maximise comfort and minimise weight. It was packaged with the break leaver, horn button, speedometer and throttle. The transparent polycarbonate aeroshell and a pair of rear-view mirrors were put in place to ensure the visibility requirements were met.

The final task was to consider the safety and comfort of the driver. A 5-point harness was integrated with the chassis to ensure proper load distribution and a horn was added to avoid collisions. The team then worked alongside the Chassis team in order to combine the side supports of the chassis with the seat. A ventilation system was designed in conjunction with the visibility holes for the horn and a hydration system was also included.

Please refer to the reports by Matilda Cole and Tianyi Sun for detailed information on ‘Driver Environment and Interfaces’.

Vehicle Dynamics and Traction

The role of the Vehicle Dynamics subgroup in this project was to identify how the changes in various aspects of the design affect vehicle performance and stability. The main aspects were focused on include: total mass of the vehicle with the driver, drive train parameters, aerodynamic characteristics, tyre selection and tyre forces.

The initial tyre force model was created by estimating the minimum cruising speed required for the car to complete the race within the time limit set. The initial tyre force estimations were then used to validate the initial vehicle dimensions proposed by the Chassis team and it also allowed the Steering and Drive train teams to have an estimate of what the maximum required steering angle and traction force would be. Once the Chassis team was close to finalizing the vehicle dimensions, an FEA analysis was then performed using the maximum tyre loads obtained from the tyre model. A lap simulator was also created and validated in order to predict the vehicle performance based on energy consumption of the car throughout the race, which motivated the study into energy efficient driving strategies once the basic accelerating then cruising velocity profile was created as a baseline for comparison. The lap simulator script which was written in MATLAB was later put together with the other sub-teams’ scripts which output variables such as the aerodynamic and tyre forces on the car, motor power and battery simulation. Stability checks on steering, tyre grip and rollover were also included within the lap simulator to ensure final vehicle stability.

Please refer to the reports by Qirui Wang and Nicholas Tham for detailed information on ‘Vehicle Dynamics and Traction’.

Battery and Cooling

The role of the Battery and Cooling sub-team was to design an electrical energy storage unit capable of storing and releasing the required energy during the race; this was found to be 35 Wh, with an output-voltage > 15 V and current up to 10 A. The use of Lithium-ion batteries, capacitors and structural batteries were considered; however, latter was ruled out by the regulations and it was found that using Lithium-ion batteries provided the lightest solution. A circuit model was produced to model the battery discharge which was incorporated the drivetrain and motor controller. A battery management system was configured and metal tray incorporated into the casing to meet the required regulations.

Final estimation of the power consumption was 15 Wh. Hence, a smaller battery would suffice, now limited by the voltage requirement. This would result in a 120 g weight reduction. However, this reduction can also be realised, without capacity loss, by using higher capacity cells at the additional cost of £27. IRG required the vehicle temperature to remain below 40°C. To estimate the vehicle temperature the heat transfer modes were modelled in the worst-case scenario (no wind, $T_a = 30^\circ\text{C}$, $T_{track} = 60^\circ\text{C}$). The main heating effects were found to be solar gain and driver heat. To mitigate these effects a reflective film covering with low absorbance was used and a ventilation inlet was sized at 1600 mm². Future recommendations include decreasing the absorbance by tinting of and/or reducing the size of the window as well as looking into the possibility of making the driver more comfortable at hotter temperatures allowing higher temperatures, resulting in a reduction of the inlet size and thus drag.

Please refer to the report by Gregorius Campman for detailed information on ‘Battery and Cooling’.

CAD and Integration

The role of CAD & Integration team is to build a CAD model of the car and update it weekly. The CAD models were generated in Solidworks 2019 and were used to visualize each component, check the compatibility of each component, optimize space and calculate the center of gravity. This ensures the chassis would not stick out of the shell, front wheels would not touch anything while turning and enough space was designed for the driver to comply with the regulations, etc.

Since a CAD model is essential for CFD analysis, we work closely with *Aerodynamics Team* to keep updating the model of the shell. We started from a rough design with only top and side view to a complete aeroshell design with wheel fairings. Also, we work closely with *Chassis Team* to update the model from a simple plate

to a 3D space frame to give the team a general concept of the car at every stage. By working with *Steering, Braking, Drive Train, Battery and Driver Interference Team*, all components were packed within the confines of the shell.

Please refer to the reports by Yuheng Wang and Yueqing Yang for detailed information on ‘CAD & Integration’.

Component	Description
Aerodynamic shell	Custom top, side and under-body profiles with integrated wheel fairings produced from CFRP and a Polycarbonate canopy
Wheel layout	2 x front wheels (steering) and 1 x rear drive wheel
Steering	Front wheel Ackermann steering, handlebar operation, pitman arm and tie rod connection under chassis floor
Motor	180 W Brushless Maxon 574741
Battery	8 x Samsung INR18650-25R cells (3.6V)
Tyre	Michelin Prototype 45/75R16
Wheels	Alienation TCS VANDAL rim + Shimano RS770 hub
Brakes	3 x BR-M8110 brake callipers
Roll bar	Aluminium Alloy 2090 T83 roll bar
Chassis	Spaceframe configuration consisting of roll wrapped CFRP tubes, with Al-6082-T6 inserts bonded together by Excel HexBond 870 A/B Shimming epoxy
Controller	Maxon Escon 70/10
Suspension	None

Table 1: List of main components and a brief description

Parameter	Value
Track width	632 mm
Wheel base	1616 mm
Mass (no driver)	25.493 kg
Ground clearance	160 mm
Max height	804 mm
Max length	3150 mm
Drag coefficient (ideal)	0.07562
Frontal area	0.52731
Tyre rolling resistance	0.00081
Project cost estimation	£3712.71
Performance estimation	1141.14 km/kWh

Table 2: List of key parameters and their values

2 CFD Validation

2.1 Need for CFD

Computational Fluid Dynamics (CFD) is the method by which the aerodynamics of the vehicle will be evaluated. The basic principles of automotive aerodynamics is a well understood field, with books such as [4] highlighting many of the key ones, that can allow anyone to design a relatively aerodynamic car with little effort. However, to truly optimise aerodynamic performance, one has to understand and refine 3D flow effects that is unique to each design. The current cost and in-availability of wind tunnel testing, in addition to a lack of model construction expertise, makes wind tunnel testing impractical. The versatility of CFD and its iterative capacity makes it ideal for the preliminary design. An initial design in CFD should be followed by correlation of wind tunnel performance and finally on-track performance. The chosen CFD package is STAR-CCM+ from CD-adapco. [4].

2.2 Need for Validation

Validation is the process of determining the degree to which a simulated model is an accurate representation of real-world phenomenon from the perspective of the intended use of the model [5]. Only after settings have been validated can results be used for further correlation work. CFD softwares are sometimes termed “black-boxes”, a non-subtle hint at the careless way output results can be taken at face value. Validation is the first step towards understanding what goes into a typical CFD simulation to better understand its outputs.

From the perspective of setting up a simulation, SEM vehicles are classified as a ground vehicle: a bluff body moving in close proximity to the road [5]. The approach towards validating the simulation settings of the SEM vehicle was so: Use a model that exhibits similar key flow features and simulate it in CFD under identical flow conditions to the SEM vehicle. The model should have reliable experimental data to compare key integral values. A comparison of these values will validate the degree to which these settings are representative of possible real world results.

2.3 Ahmed Body

The Ahmed body is an automotive industry standard model used for validation of ground vehicle simulations as there is a wealth of experimental data to correlate numerical solutions. The key flow feature desired during validation is the region of separated flow at the rear of a vehicle, a feature that is present in many basic vehicle shapes. There are also unsteady vortices that are shed downstream [6]. The wake structure formed contributes to the pressure drag. Therefor, the Ahmed Body exhibits an essential flow feature of a real vehicle (Excluding rotating wheels, engine

and passenger compartment flow, rough underside, and surface projections) [7]. The dimensions of the Ahmed Body can be found in the Appendix A.1. The model used has a slant angle of 25°.

2.4 Problem Definition and Boundaries

The flow conditions expected was estimated as follows. The vehicle was approximated as a simple flat plate of a maximum length of 3.5m (maximum regulation length of vehicle). Using sea-level atmospheric conditions, the Reynolds Number was approximated as 1.64×10^6 with a velocity of 7.0m/s. This velocity was the average velocity the needed to complete the circuit in time as determined by the Vehicle Dynamics Team. Refer to the Vehicle Dynamics report by N.Tham for further discussion on this.

$$Re_{length} = \frac{\rho U D}{\mu} \quad \text{and hence} \quad x_{crit} = 1.043m \quad (1)$$

Laminar, transition and turbulent flow models are available in STAR-CCM+. From literature [8], flow along a flat plate can transition from laminar to turbulent at Reynolds Numbers as low as 500,000. Assuming this low transition value and substituting it back into the equation above, yields an approximation of the transition point along the plate/vehicle, x_{crit} . Based on this conservative figure, 75% of the length of the vehicle is expected to have a turbulent boundary layer. Hence, a turbulence model will be chosen instead of laminar.

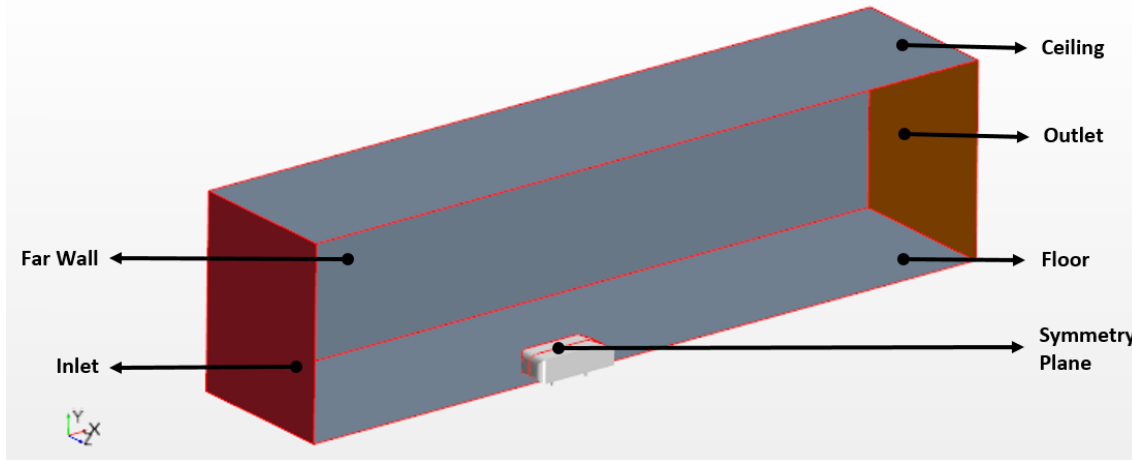


Figure 1: The computational domain for the validation of the Ahmed Body

The computational domain was set up as follows in Figure 1. The dimensions were set such that the blockage effect will be below 4%, ensuring its effects on the simulation results are minimal and can be found in the Appendix A.1. The dimensions are defined in terms of the model's length, width, and maximum height

and are similar to the virtual wind tunnel described in [7]. Since the model is symmetrical along the longitudinal axis, the computational domain was halved to save on computational time. The boundaries were named: Inlet, Outlet, Symmetry Plane, Floor, Ahmed Body, Ceiling and Far Wall. Their wall conditions are shown in Table 3.

Table 3: Summary of boundary types for Ahmed Body simulation

Boundary	Type
Inlet	Velocity Inlet
Outlet	Pressure Outlet
Symmetry Plane	Symmetry Plane
Floor, Ahmed Body	No-Slip Wall
Ceiling, Far Wall	Slip Wall

The velocity inlet was set to a velocity of 7.0m/s and the target Reynolds Number is 1.64×10^6 , similar to the expected track conditions of the vehicle. The variable used for validation was a C_D of 0.3155 obtained from the empirical relation between C_D and Reynolds Number for this model of the Ahmed Body [7]. Note that the pressure and shear forces were collected from the Ahmed Body surfaces and excluded the stilts as they provide the ground clearance[1].

2.5 Mesh Settings and Volumes of Refinement

Variation of parameters within the turbulent boundary is an important quantity to be measured, prism layers were used to allow the boundary layer profile to be accurately resolved [3]. A trimmer mesh was used as it is a popular choice when modelling external aerodynamic flows, particularly in refining and capturing wake region phenomenon [3]. It is also useful when working with imperfect CAD geometries as polyhedral and tetrahedral meshes do not form well on imperfect surface geometries [3]. Trimmer cells are computationally quicker and less memory-intensive [2]. Its poorer resolution in the wake, relative to polyhedral cells, can be compensated with a finer mesh in the wake region [2]. The surface-remesher was used to ensure coherence between the initial surface mesh and the volume mesh that grows from it [3].

Not all areas of the computational domain are expected to contain complex flow structures that warrant a finer mesh. High mesh refinement is needed in areas of complex physics, such as around the body, legs, and wake. This method of selective mesh refinement further reduces the cell count and saves on computational time. Two methodologies allow for this: Volumetric Control and Constant Mesh Growth Rate. An explanation of their differences can be found in Appendix 9. The Volumetric Control method was chosen after several trial meshes were performed that showed it provided far better mesh control. Volumetric Control provides far bet-

ter accuracy than constant growth rate [2] and is best illustrated in Appendix A.6. For dimensions of the Volume of Refinement and Computational Domain, refer to Appendix A.1 and A.2

2.6 Physics Settings

The segregated solver is suitable for problems involving in-compressible and low Mach flow and it requires much less memory. Using the default All Y+ Wall Treatment model, several meshes were performed to tune the prism layer thickness to obtain the appropriate range ($Y+ \leq 1$ or $Y+ \geq 30$). The two turbulence models tested were the $k-\omega$ SST and the Two-Layer $k-\epsilon$, with the latter being the recommended model by STAR-CCM+ [3]. It was postulated that $k-\omega$ SST will be the better option due to its ability to predict separation and reattachment better when compared to $k-\epsilon$ and the standard $k-\omega$. It marries the $k-\epsilon$ and $k-\omega$ models, working like $k-\epsilon$ in the far field and $k-\omega$ near the target geometry [3]. Due to the unsteady vortices expected to be shed, the steady and unsteady time settings tested.

Table 4: *Effect of changing turbulence model and solver state on drag coefficient prediction*

Turbulence Model	Time	Convergence	Error	C_D
Two-Layer $k-\epsilon$	Steady	2850 iterations	-5.3%	0.2988
Two-Layer $k-\epsilon$	Un-Steady	No Convergence	-5.9%	0.2969
$k-\omega$ SST	Steady	2250 iterations	-2.7%	0.3071
$k-\omega$ SST	Un-Steady	No Convergence	-3.4%	0.3048

The results from Table 4 show an under-prediction of the drag coefficient across all settings. $k-\omega$ SST provides a slightly higher level of accuracy in both the steady and un-steady simulations. All cases were ran at a mesh size of 2.7 million and for 5000 iterations. For steady state simulations, convergence was seen when periodic oscillations about a mean value was observed as iterations increased. For unsteady state simulations, oscillations displayed no indications of periodicity. A crude approximation for the mean value of the drag coefficient was obtained to establish an error percentage. For plots of the integral values and residuals, refer to Appendix A.4. Using these approximations, the steady state simulations were also marginally more accurate than the unsteady states. Unsteady simulations also typically take an order of magnitude longer to converge. Hence, a steady state $k-\omega$ SST turbulence model was chosen.

2.7 Convergence

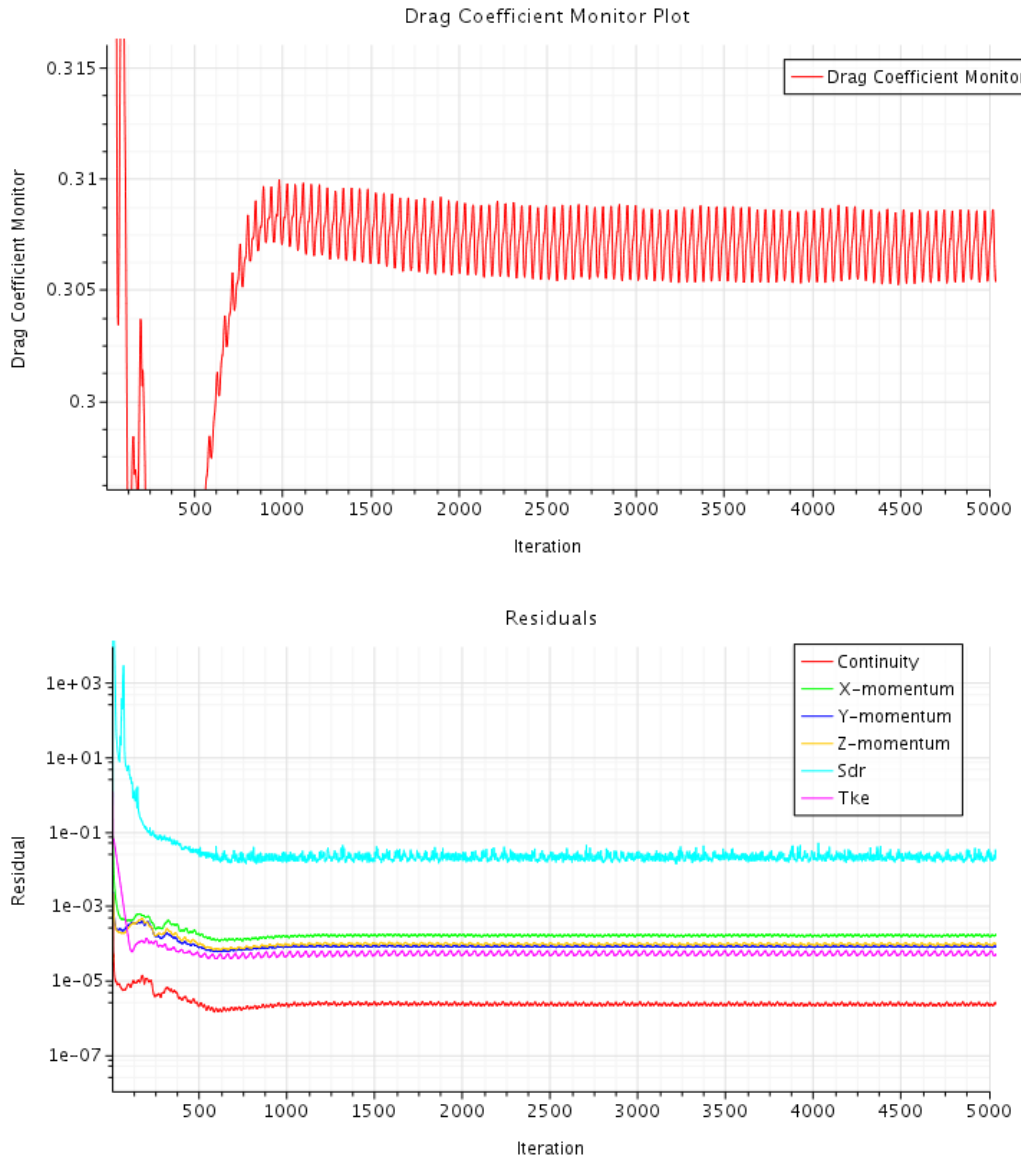


Figure 2: Periodic oscillations about a mean value observed in the Drag Coefficient from a steady $k - \omega$ SST simulation of the Ahmed Body

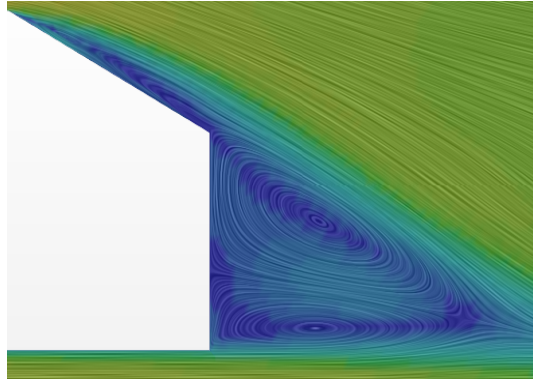
Convergence of the numerical solution can be difficult to define. The default settings in STAR-CCM+ suggest residual values of 1.0×10^{-4} to signify a converged solution. Following consultation with Dr George Papadakis and a former GDP student, the measure of convergence was set as having all residuals decrease by at least 3 orders of magnitude from their initial values and a general plateauing or periodic oscillations about a mean value of the integral values. This criteria was used to evaluate the simulations in Section 2.6. Note from the residual plot in Figure 2, only the Sdr residual is unable to hit this criterion. Efforts to investigate different settings to obtain convergence were eventually abandoned to focus on the 3D analysis of the SEM shell.

2.8 Results

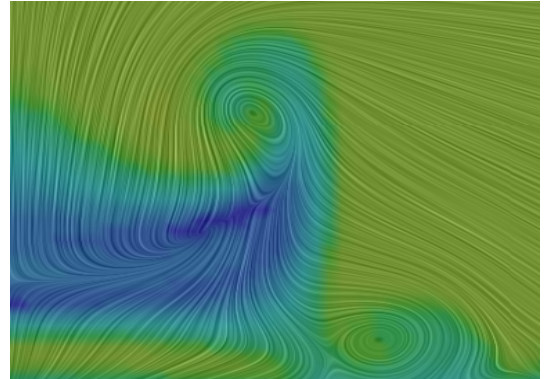
Table 5: Validated settings

Governing Equation	Turbulence	Time	Solver	Wall Treatment	Mesher
Constant Density RANS	$k - \omega$ SST	Steady	Segregated	All Y+	Trimmer Cells Prism Layers S.Wrapper S.Remesher

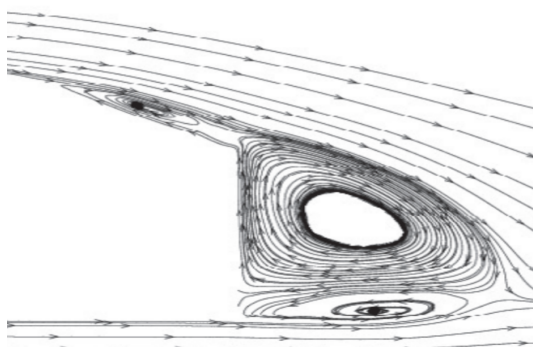
Figure 3 shows the comparison of the wake structure between simulation and literature. The two unsteady vortices that is characteristic of the wake was captured in both steady and unsteady state simulation. The shape of these vortices were similar with those from higher fidelity simulations performed in [1].



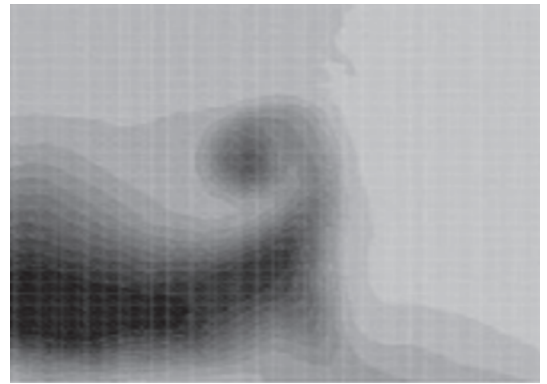
(a) Side wake profile from simulations



(b) Rear wake profile from simulations



(c) Side wake profile from [1]



(d) Rear wake profile from [1]

Figure 3: The side and rear wake profile from the simulation matches that from a Large Eddy Simulation from [1]

3 Preliminary Designs

3.1 SEM simulation

The set-up of the SEM vehicle simulations are similar to that of the Ahmed Body. Refer to Appendix A.5 for images of the mesh and domain. A minimum mesh size of 2.7×10^6 was found to allow good quality prism layers to form.

3.2 Mesh Independence Study

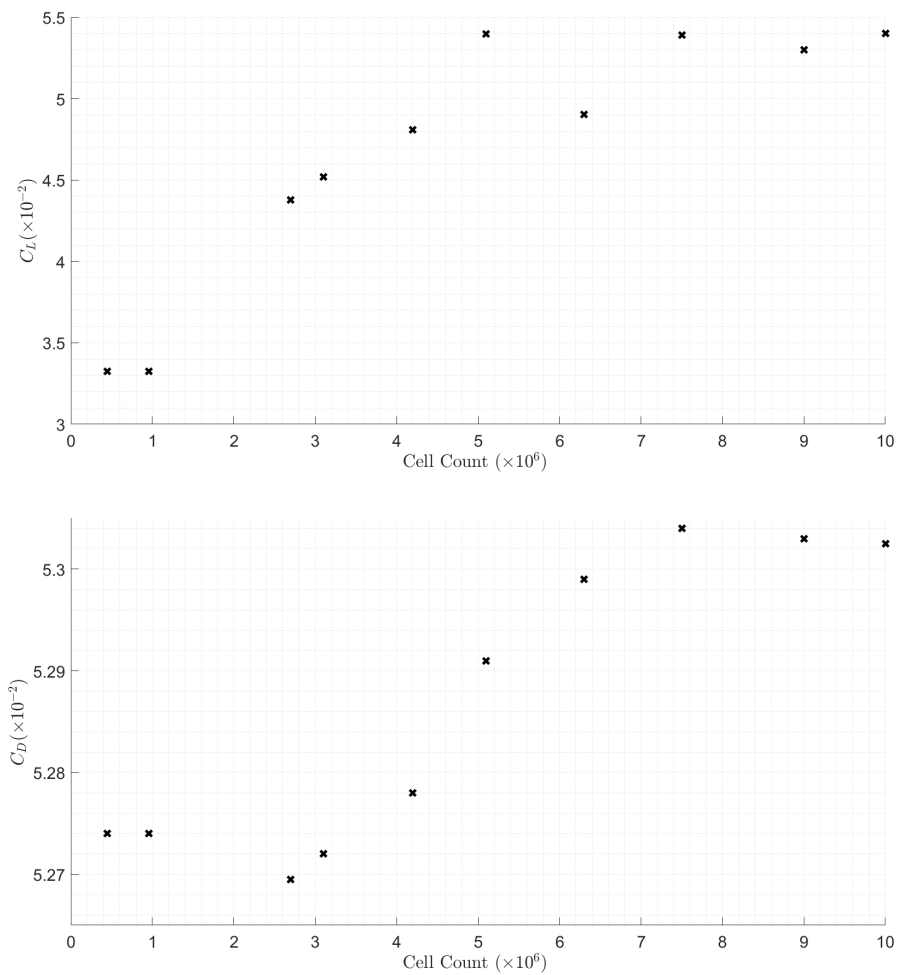


Figure 4: Plots showing the variation of C_L and C_D with increasing cell count.

Integral values increase with mesh size. Therefore, finding the mesh size at which the integral values are independent of the mesh is known as achieving mesh independence. Mesh independence is unique to each set-up and flow field and provides users with the optimal mesh size for accurate results without excessive computational time. It provides an understanding of the associated mesh-dependent error in values should simulations be limited by memory constraints and processing power.

The set-up described in Section 3.1 was tested at various cell counts and the variation in C_d and C_l plotted in Figure 4. Due to the limited processing power of personal computers and the large volume of jobs being ran on Imperial College's Hurricane and Spitfire servers, mesh independence testing was limited to approximately 10 million cells. From the available testing data, mesh independence for the SEM set-up occurs at approximately 7 to 8 million cells. For the purpose of accuracy and maintaining good simulation practice, it was recommended that all simulations should be performed at mesh-independent cell counts. Given hardware and time constraints, the simulation run times in Table 6 were considered. Running at a 2.7 million cell count produces a mesh dependent error of 0.5% and 23.6% for C_D and C_L . Keeping the primary goal of reducing C_{DA} in mind, the low error in C_D and increase in run time of almost 10 hours at mesh independent size justified running all further simulations at 2.7 million cells.

Table 6: *Difference in speed of simulation at mesh independent and dependent cell count.
Simulations performed on a 4 core Intel i7-7500U CPU*

Cell Count	Mesh Independence	Seconds per iteration	Run Time (Hours)
2.7×10^6	No	7	3 to 4
9.0×10^6	Yes	25	10 to 14

3.3 IRG Aeroshell Appraisal

Table 7: *Comparison of drag coefficient predictions for the IRG 2019 shell*

Simulation	C_d	C_l	C_{dA}
OpenFOAM	0.1342	0.186	0.0477
STAR-CCM+	0.0826	-0.329	0.0293

With the goal of creating a design that matches or surpasses IRG's current design, it was imperative to run a simulation using the validating settings from Section 2.8. Prior to this project, a simulation was performed in OpenFOAM by Mr Tomas Mrazek, the results of which were made available in [9]. The large differences in values brought scrutiny over the validated settings and will be a point of improvement. Despite the differences, the C_d value of 0.0293 was the value to beat.

3.4 Iteration One

For the first design iteration, the focus was on testing the effects of 3 different wheel fairing designs: Non-cambered, Cambered and Dual Tapered Fairings. The results are presented in Table 8.

Table 8: Results of the simulations performed on the 3 wheel fairing designs

Wheel Fairing	Frontal Area (m^2)	C_d	C_l	C_dA	C_lA
Non-Cambered	0.4831	0.0801	0.0670	0.0387	0.0324
Cambered	0.4853	0.0796	-0.0103	0.0386	-0.0050
Dual-Tapered	0.4763	0.0796	0.0639	0.0379	0.0305

Review

1. A non-cambered wheel fairing design results in positive lift of the vehicle
2. Cambering counters the production of lift without significantly altering C_dA
3. Reduction in C_dA from a Dual-Tapered design comes from the decrease in frontal area rather than a change in C_d . This design produces positive lift

Result of first iteration

Future design iterations now had cambered front wheel fairings to obtain as neutral lift as possible. The decision was made following an initial guidance by the Vehicle Dynamics team concerning the potential destabilising effects of positive lift on stability, particularly during a bank. Refer to the Vehicle Dynamics report by N.Tham for further discussion.

3.5 Iteration Two

The focus was on the testing the effects of vehicle length on the aerodynamic performance. The length of the vehicle was controlled by the thickness-to-chord ratio of the top profile aerofoil. As the maximum thickness of the vehicle was a constant, shortening the length resulted in a larger thickness-chord ratio and vice versa. A longer length was set as 3.45m and the shorter at 3.0m. This gave thickness-chord ratios of 27.6% and 31.7% respectively. The base aerofoil was a GOE-776 and was altered to fit obtain these thickness-chord ratios. For more information refer to the Aerodynamics report by M.Wietlicki.

Table 9: Results of the simulations performed on different vehicle lengths

Vehicle Length	Frontal Area (m^2)	C_D	C_L	C_{DA} (m^2)	C_{LA} (m^2)
3.45m	0.5326	0.0822	0.0048	0.0438	0.0025
3.00m	0.5233	0.0840	0.0550	0.0440	0.0288

Review

1. A shorter length results in an order of magnitude increase in positive lift
2. $C_D A$ remained relatively unchanged using this methodology. Hence it was not used as the deciding factor for this iteration

Result of second iteration

With a significant reduction in side profile area from a shorter length, this could significantly improve the crosswind performance of the vehicle. Side forces will be smaller with a smaller side profile area. Guidance by the Vehicle Dynamics suggested that excessive side forces can contribute to instability. Hence, the decision was made to minimise the side profile area to minimise the side force produced during a crosswind by selecting the shorter vehicle length.

At this stage of the preliminary design, Vehicle Dynamics communicated the relaxing of constraints on positive lift, after further analysis of the dynamics. Hence, the positive lift penalties from a shorter vehicle were less of a consideration in this design choice. Future design iterations can be performed to reduce positive lift. This is explored further in the Aerodynamics reports of T.Bryce-Smith, C.van den Berg and M.Wietlicki.

4 Final Design

4.1 Results

In the final week of the project, a decision was made to shorten the wheel base and widen the chassis. The result was the bottom roll bar protruding from the latest shell design. The time constraint and the complexity involved in selecting reshaping and remodelling the shell in CAD were challenging. A simple scaling of the final shell by +5% was performed in order to meet the new constraints. This scaled shell became the final design. CFD simulations were performed at a mesh independent cell count for the first and final iteration and the results are presented in Table 10.

Table 10: Results of mesh-independent simulations of final (red) and first design. Also included are the results of the final shell without the scaling performed

Design	Frontal Area (m^2)	C_D	C_L	C_{DA} (m^2)	C_{LA} (m^2)
Final (Scaled)	0.5273	0.0756	0.1152	0.0399	0.0608
Final	0.4688	0.0753	0.0811	0.0353	0.0380
First	0.4853	0.0796	-0.0103	0.0386	-0.0050

The poorer performance in C_{DA} was expected surprising. While the efforts to reduce drag had yielded a 5.2% reduction in C_D , the scaling performed had increased the frontal area by 8.7% instead, leading to an overall increase in C_{DA} . The design also shifted from a negative/neutral lift to a positive lift. Nevertheless, the shell's flow features analysed and suggestions were made to mitigate undesirable flow features. Refer to the Aerodynamics reports of T.Bryce-Smith, C.van den Berg and M.Wietlicki for further analysis. Also presented in Table 10 are the simulation results for the un-scaled final shell design as comparison.

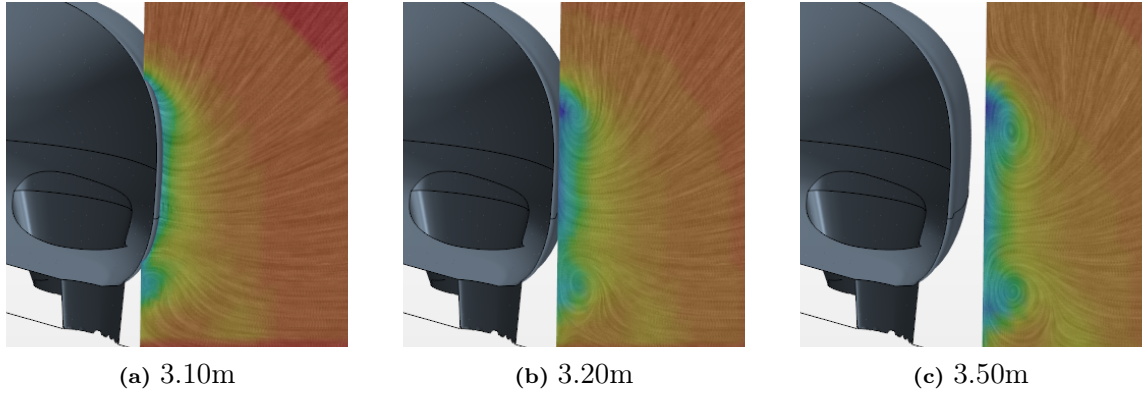


Figure 5: A line integral convolution (LIC) of the velocity vectors was taken at three locations from the nose of the vehicle

From Figure 5, two vortices formed along the rear of the vehicle. The formation of these are characteristic of bluff vehicle flows as mentioned in Section 2.2. The use of the Ahmed Body to validate CFD settings required to model this feature is hence justified. Although not available in this report, a similar LIC of the velocity vectors for the side profile of the vehicle showed no vortices similar to those seen in Figure 3. This was probably due to the gentle gradient on the rear of the SEM vehicle compared to the 90° surface on the rear of the Ahmed Body.

4.2 Future CFD Considerations

1. Further validation of STAR-CCM+ settings

While validation of the Ahmed Body yielded a low error in C_d of 2.7% , the disparity in drag predictions for IRG shell in Section 7 is a cause of concern. Discussing the various settings used by Mr Tomas Mrazek yield no conclusion to the reason for the disparity. IRG's CFD analysis was validated against drag values of PAC Car II by ETH [9]. As the PAC Car II's drag coefficient was obtained via wind tunnel testing [10], it is concluded that IRG's results are more representative of real world performance in a wind tunnel. While the integral values obtained were used to compare performances between designs, further

validation work must be performed in STAR-CCM+ before it can integrated into IRG's design process.

2. Higher priority on rotating wheel simulations

The rotation of the wheel contributes a significant amount of drag making the wheel fairings an almost non-negotiable design feature. Despite this, the final design still has the bottom of the wheels exposed for a height of approximately 40mm. Researchers and racing teams dedicate tremendous resources to understanding, reducing and manipulating the wheel wake to improve drag performance. Rotating wheels and their housing can contribute to as much as 25% of drag in modern vehicles and more crucially interacts with under-body flow and the wake [11]. The loss manpower in the CAD team and time constraints of the project undermined the goal to simulate this crucial boundary condition. Future students working simulations should place this at the forefront of their priorities.

3. Cross-wind performance

Simulations performed in this project have been strictly confined to head-on flow. The various turns and unpredictable environment makes a head-on flow highly unlikely. Efforts were made to attempt a cross-wind simulation of the flow. The complexity of the flow, possibly incorrect boundary conditions and computation domain sizing made a converged solution impossible. A similar investigation was performed by M.Wielicki.

4. Time-based simulations

To further understand the real world performance of the car, time-based simulations can be performed. This will involve a time-varying wing angles and velocities that will be expected to be seen by the vehicle on track. This will involve closer collaboration between the Vehicle Dynamics team and the Aerodynamics team.

5 Conclusion

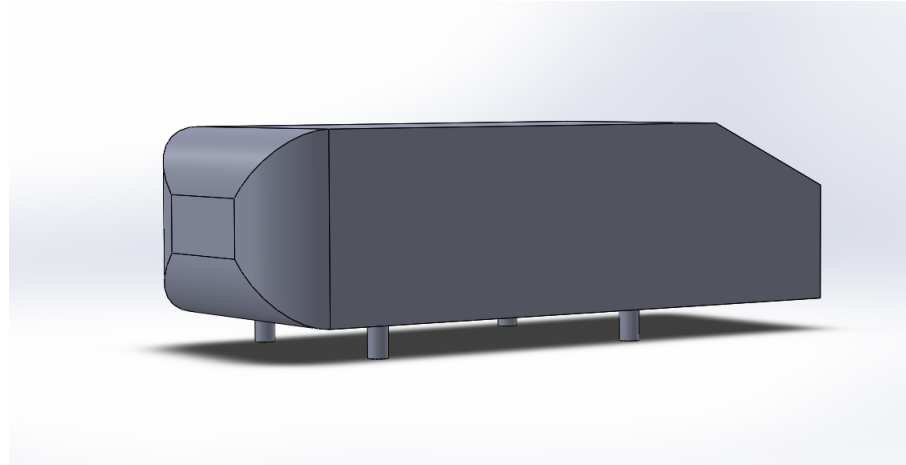
In this five weeks, CFD settings were validated on an Ahmed Body, with an under prediction of -2.7% of the empirical drag coefficient. All subsequent simulations used a steady-state $k - \omega$ SST turbulence model. Two design iterations were performed that evaluated 3 different wheel fairing designs and the effects of vehicle length on the aerodynamic performance. Despite disappointing final results, this project provides a direction for future students to familiarise with and integrate STAR-CCM+ into their design process.

References

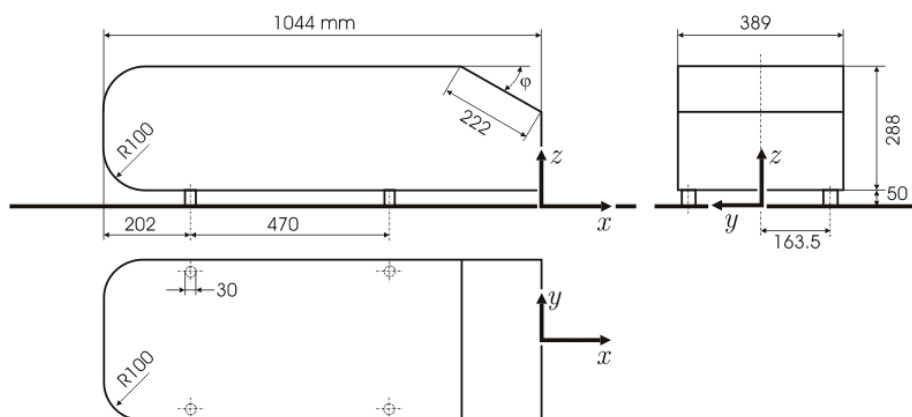
- [1] E. Serre, M. Minguez, R. Pasquetti, E. Guilmineau, G.B. Deng, M. Kornhaas, M. Schäfer, J. Fröhlich, C. Hinterberger, and W. Rodi. On simulating the turbulent flow around the ahmed body: A french–german collaborative evaluation of les and des. *Elsevier Journal of Computer & Fluids*, 78(1):10–23, 2013.
- [2] A.H. Nor, E. Abo-Serie, and A. Gaylard. Mesh optimization for ground vehicle aerodynamics. *Innovative Space of Scientific Research Journals*, 2(1):54–65, 2010.
- [3] Siemens PLM Software. *Simcenter STAR-CCM+® Documentation Version 2019.2*, 2013. Available from: Resource provided by Dr Joaquim Peiró [Accessed: 12th June 2020].
- [4] J Katz and T Kurfess (ed.). *Automotive Aerodynamics*. John Wiley & Sons, Chichester, United Kingdom, 2016. ISBN: 9781119185734.
- [5] American Institute of Aeronautics and Astronautics. *Guide for the Verification and Validation of Computational Fluid Dynamics Simulations*, 2013. Available from: <https://arc.aiaa.org/doi/abs/10.2514/4.472855> [Accessed: 12th June 2020].
- [6] S.R. Ahmed, G. Ramm, and G. Faltin. Some salient features of the time-averaged ground vehicle wake. *Society of Automotive Engineers*, 1(1):1–34, 1984.
- [7] W. Meile, G. Brenn, A. Reppenagen, B. Lechner, and A. Fuchs. Experiments and numerical simulations on the aerodynamics of the ahmed body. *Innovative Space of Scientific Research Journals*, 3(1):32–39, 2011.
- [8] J.L. Plawsky. *Transport Phenomena Fundamentals*. CRC Press Taylor & Francis Group, Boca Raton, Florida, United States of America, 2014.
- [9] S Tam, M Mahmoud, C Firgau, A Pathak, S Khan, A Vivekanandan, and T Mrazek. *Imperial Racing Green Mid-Year Report 2019-2020*. Technical report, Energy Futures Lab, Imperial College London, 2020.
- [10] JJ Santin, C Onder, J Bernard, D Isler, P Kobler, F Kolb, N Weidmann, and L Guzzella. *The World’s Most Fuel Efficient Vehicle*. VDF Hochschulverlag AG an der ETH Zürich, Zürich, Switzerland, 2007.
- [11] O.F Cavusoglu. *Aerodynamics Around Wheels and Wheelhouses*. Master’s thesis, CHALMERS UNIVERSITY OF TECHNOLOGY, Gothenburg, Sweden, June 2017. Unavailable.
- [12] S. Kumar. *Ahmed Body files and renderings*, 2014. Available from: <https://grabcad.com/library/ahmed-body-2> [Accessed:14th June 2020].

A Appendix

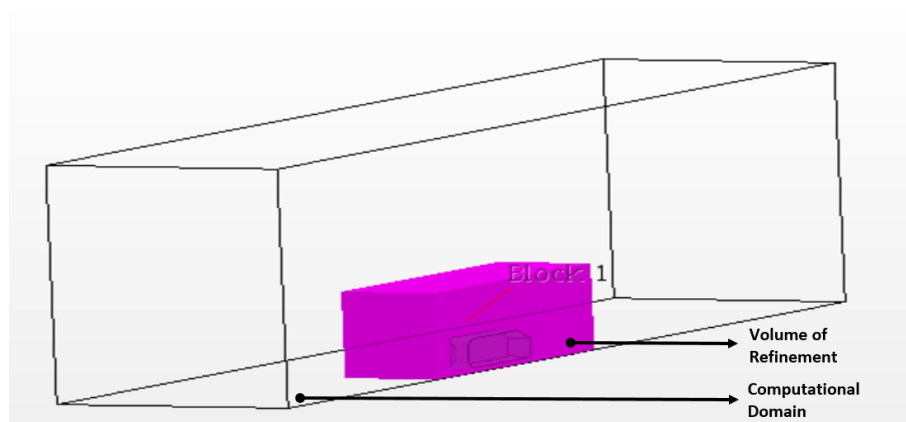
A.1 Ahmed Body



(a) Ahmed Body with 25° slant angle. Part file and rendering obtained from [12]



(b) Dimensions of the Ahmed Body. Drawing obtained from [12]



(c) Computational Domain and Volume of Refinement

Figure 6: The Ahmed Body's dimensions and placement in the computational domain

A.2 Simulation setup dimensions

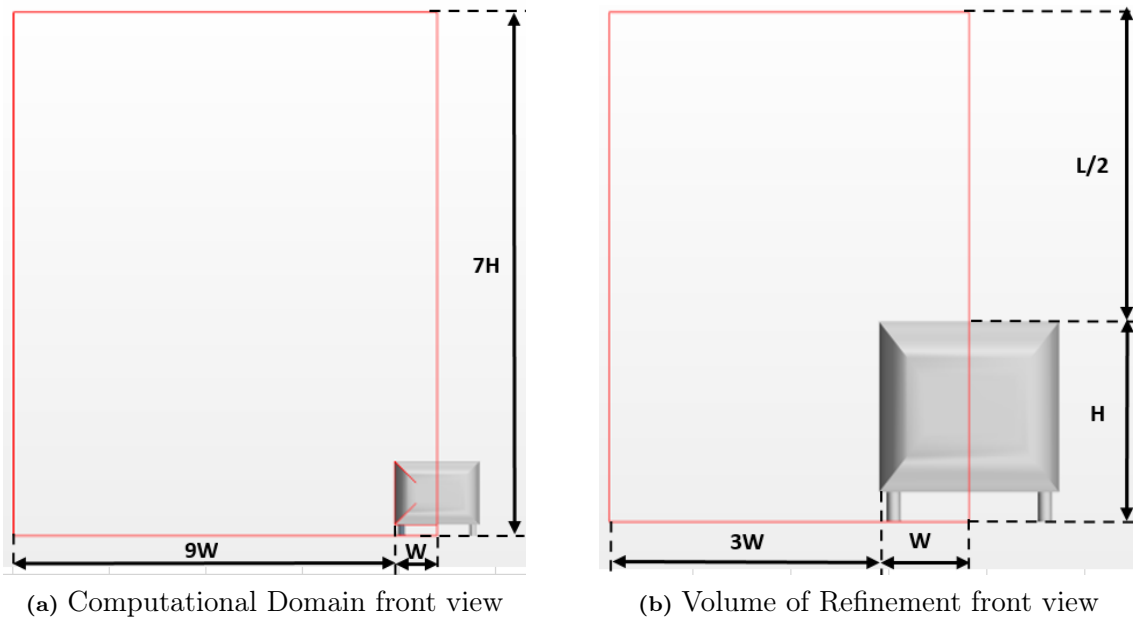


Figure 7: Dimensions for Computational Domain and the Volume of Refinement as seen from the front

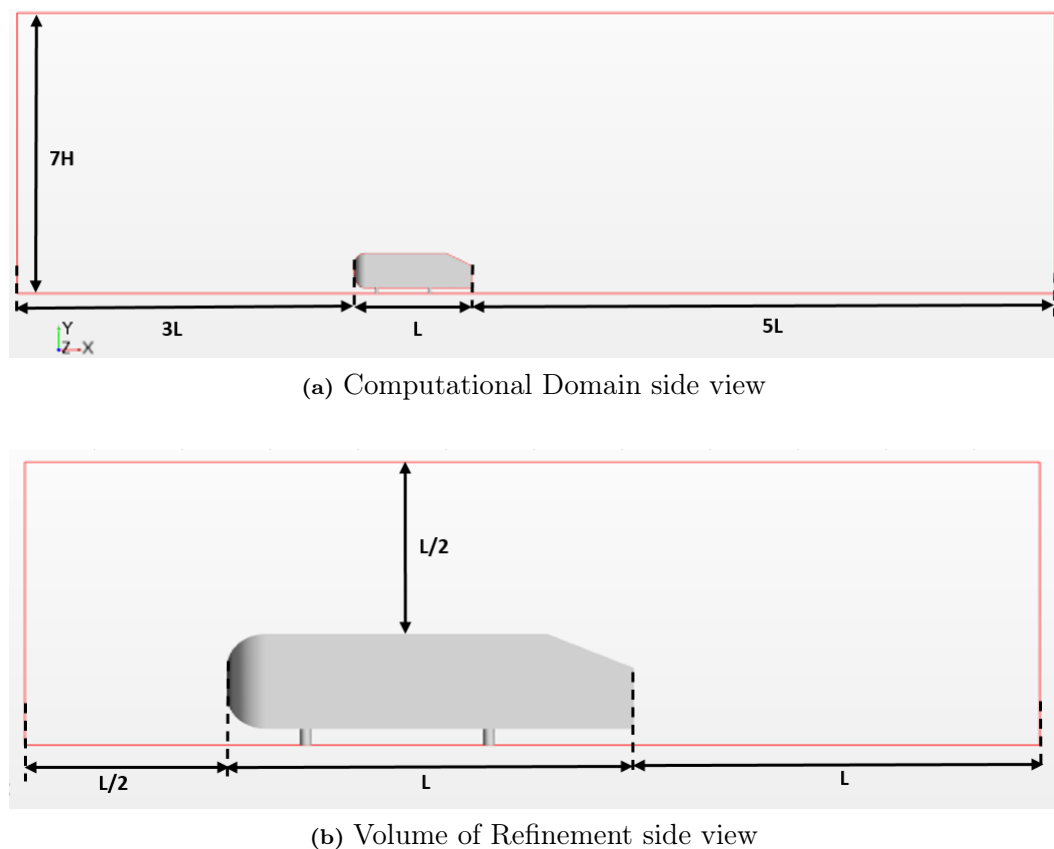


Figure 8: Dimensions for Computational Domain and the Volume of Refinement as seen from the side

A.3 Mesh Control

Table 11: *Mesh Refinement Methodologies [3]*

Method	Methodology
Volumetric Control	This allows a smaller block around the body with finer mesh to be defined by the user. The mesh then grows coarser towards the boundaries/edges of computational domain
Constant Mesh Growth Rate	Setting the mesh to grow bigger as it moves outward to the far field, at a constant growth rate

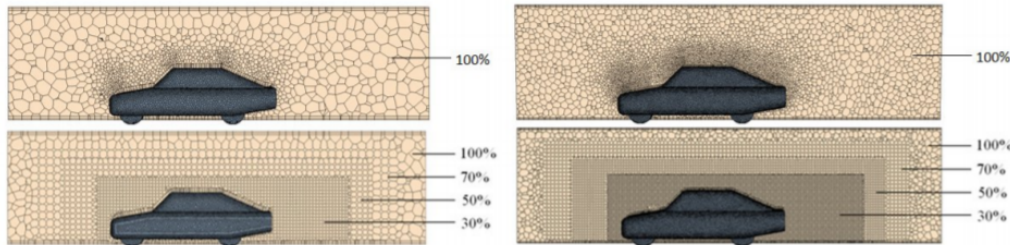


Figure 9: The degree of control over mesh refinement afforded by volumetric control is clearly demonstrated in the second row of images. The first row demonstrates how inconsistent and unpredictable the constant growth rate method can be [2]

A.4 Ahmed Body Validation Plots

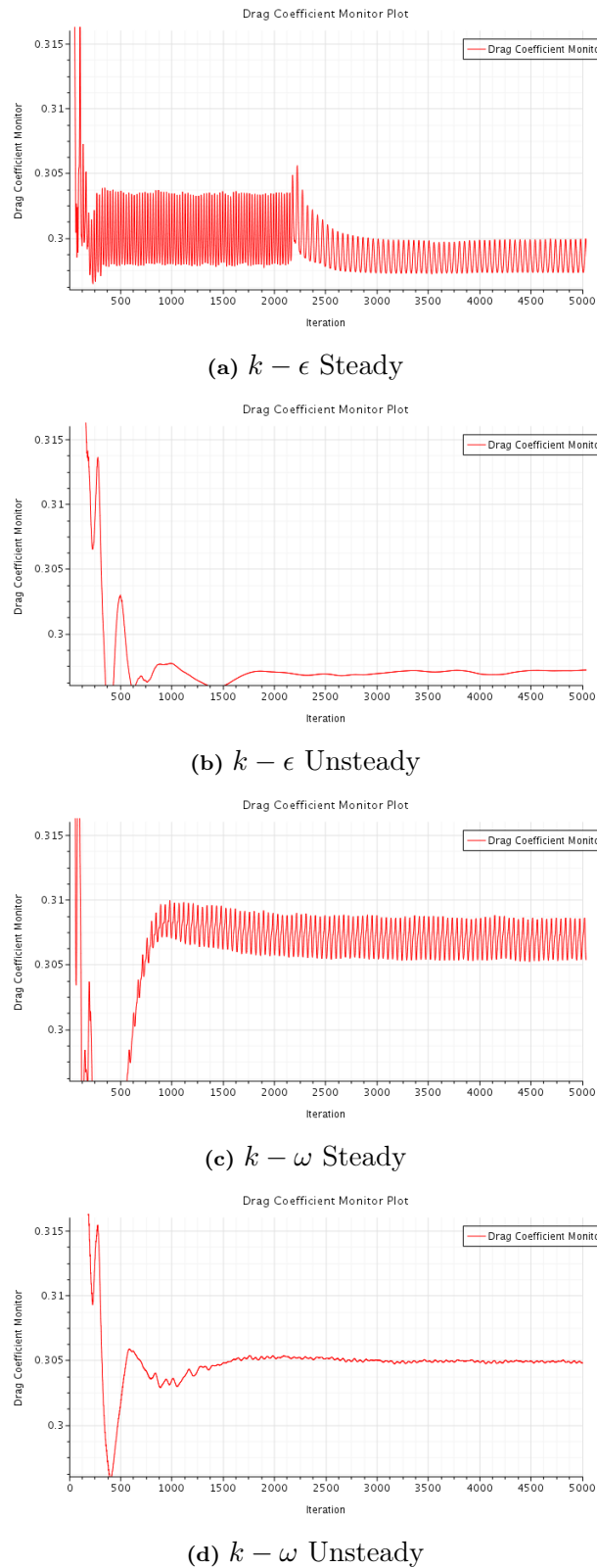


Figure 10: Drag Coefficient plot for the 4 settings

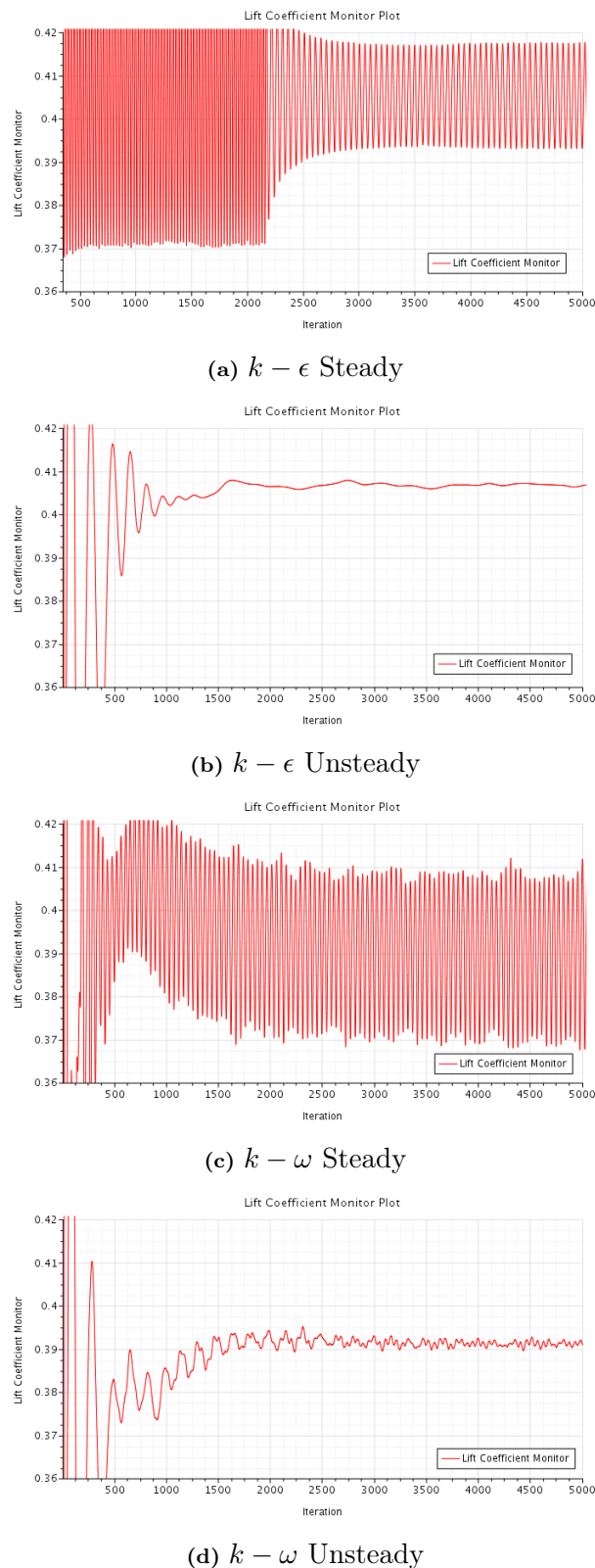


Figure 11: Lift Coefficient plot for the 4 settings

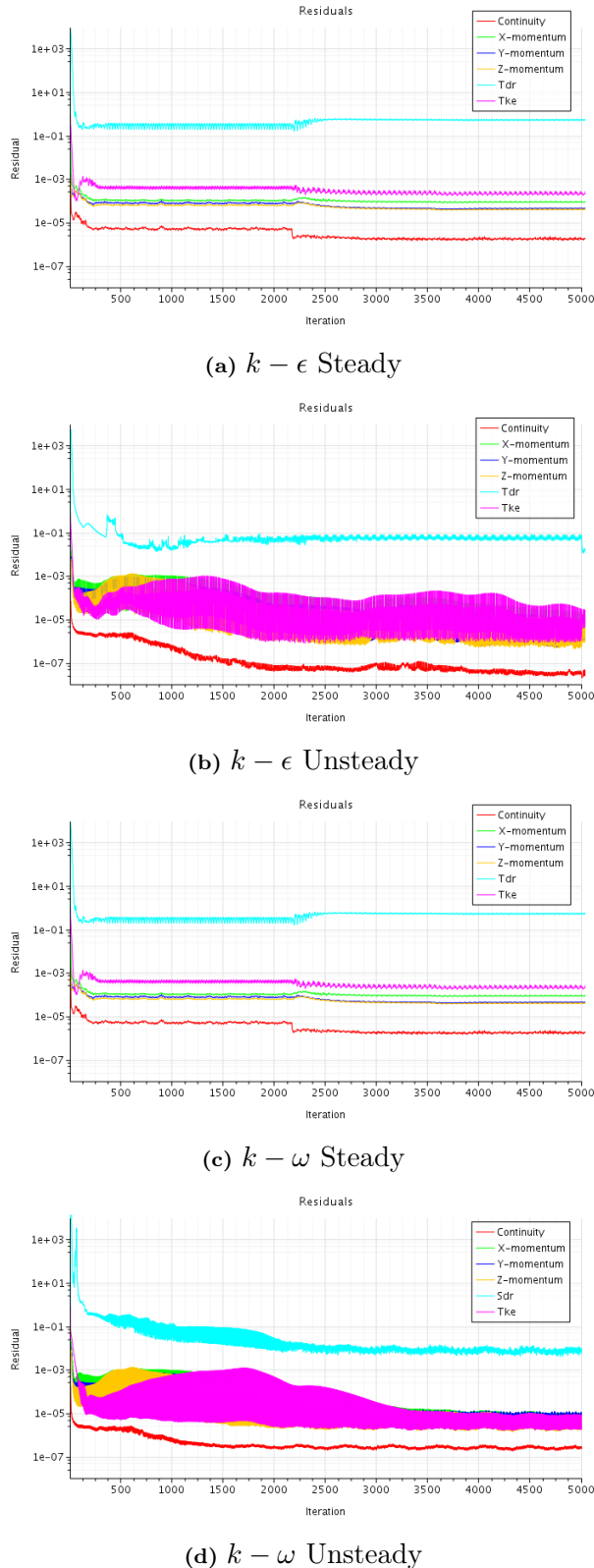


Figure 12: Residual plot for the 4 settings

A.5 SEM Simulation

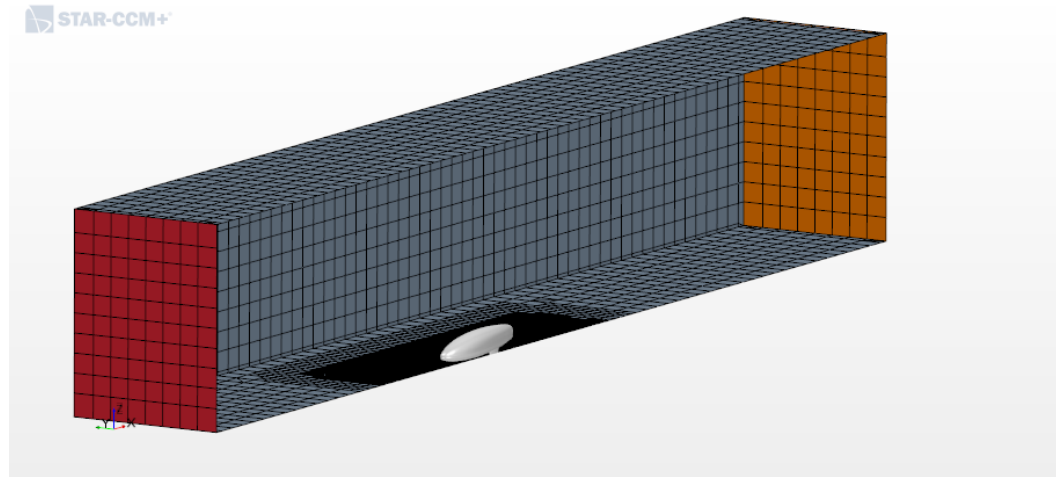


Figure 13: *The computational domain for all SEM simulations*

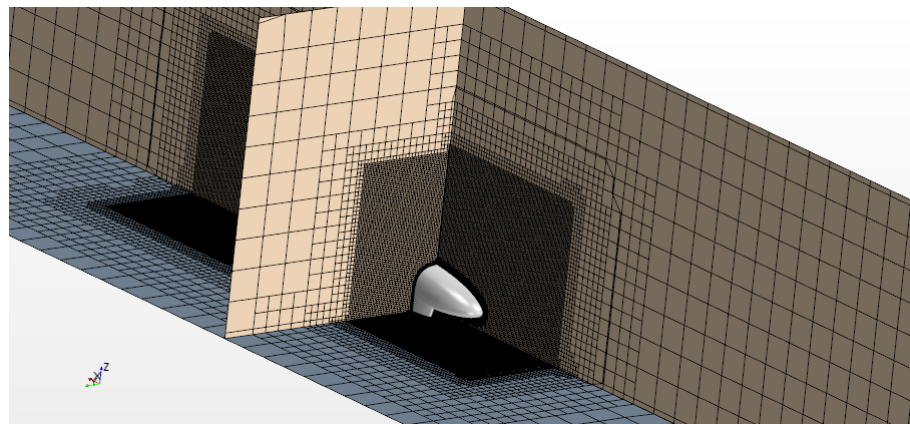


Figure 14: *The volume mesh of the SEM simulations*

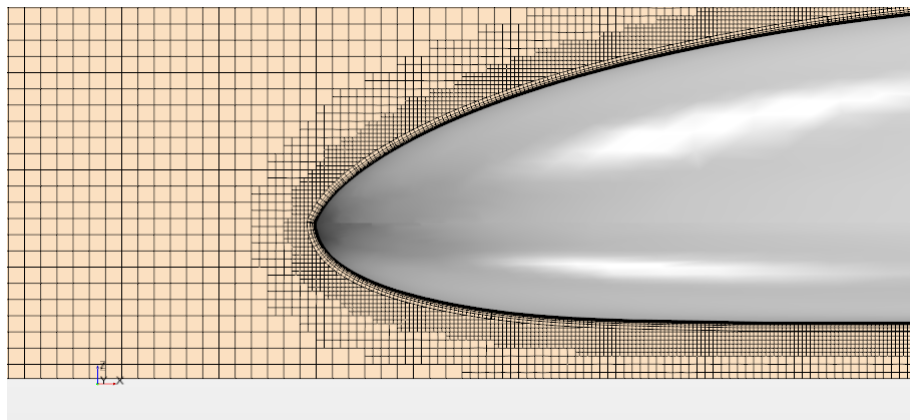


Figure 15: Prism Layers on the surface of the SEM model

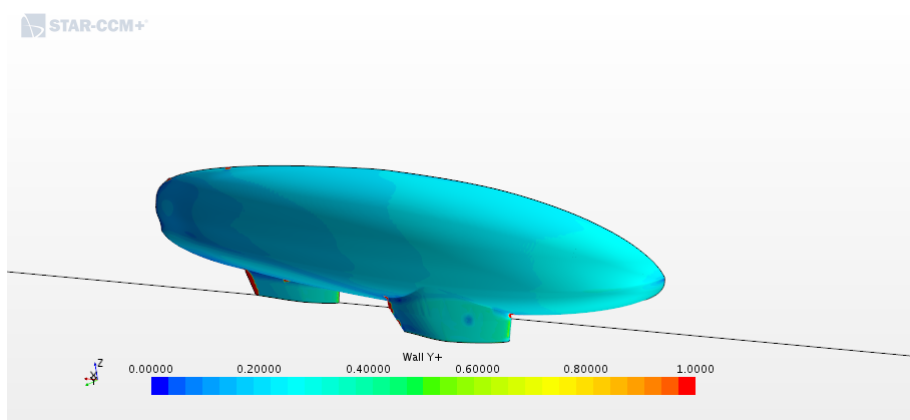


Figure 16: Wall $Y+$ values that are within range across the model

A.6 Mesh Independence

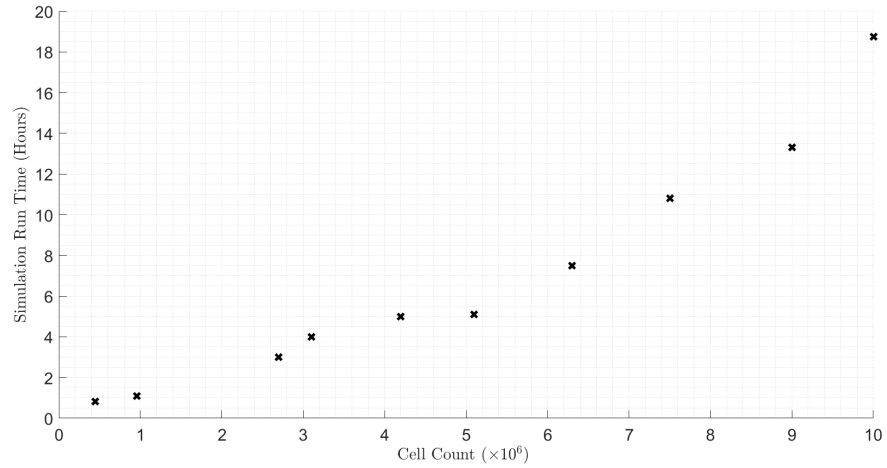


Figure 17: Plots showing the variation in total run time to convergence for the SEM setup during mesh independence test